Single-walled carbon nanotube growth from a cap fragment on an iron nanoparticle: Density-functional tight-binding molecular dynamics simulations

Yasuhito Ohta,[1] Yoshiko Okamoto,[1] Stephan Irle,[1,2,*] and Keiji Morokuma[1,†]
[1]*Fukui Institute for Fundamental Chemistry, Kyoto University, Kyoto 606-8103, Japan*
[2]*Department of Chemistry and Institute for Advanced Research, Nagoya University, Nagoya 464-8602, Japan*
(Received 8 January 2009; revised manuscript received 8 April 2009; published 14 May 2009)

Growth of a single-walled carbon nanotube (SWNT) from a corannulene cap fragment on an iron cluster is demonstrated using density-functional tight-binding molecular dynamics simulations of laser synthesis. In order to explore multiple reaction pathways for the cap fragment to evolve into tubular form on the iron surface, reaction dynamics between the metal-bound cap fragment and gas-phase carbon atoms were investigated. It is found that rapid growth of the cap fragment can take place when carbon atoms are supplied in the vicinity of the cap fragment. In this reaction process, a high-density supply of add atoms leads also to rearrangements of existing sp^2-carbon-cap structures involving the formation of pentagons and heptagons as long-lived defects, while short-lived four- and eight-membered rings and short polyyne chains appear during the dynamics as important intermediate structures, facilitating growth.

DOI: 10.1103/PhysRevB.79.195415 PACS number(s): 61.48.De, 71.15.Pd, 81.16.Dn, 82.40.Ck

I. INTRODUCTION

Despite considerable recent improvements in the metal-catalyzed production of single-walled carbon nanotubes (SWNTs) with specific desired characteristics,[1–5] complete control of their structural parameters chirality,[3] diameter,[4] and length[5] at the time of synthesis remains elusive. Recent remarkable *in situ* microscopic [environmental TEM (ETEM)] studies of Fe-catalyzed[6] and Ni-catalyzed[7] SWNT nucleation and growth showed the metal particles in action during the SWNT nucleation and growth. However, even the fastest recording speed of such ETEM movies is presently only around 30 frames per second,[7] prohibiting the observation of key events during the SWNT nucleation. Moreover, experimental findings appear to be contradictory and/or highly system dependent, in particular regarding carbide formation and the melting of the metal nanoparticles (NPs). The SWNT growth parameter space (metal catalyst composition, NP preparation, size and distributions, nature of substrates or floating catalyst, carbon source, gas flow rates, environmental temperature, inert gas type and pressure, etching addends, contaminations, etc.) is too large to be systematically fully explored, and thus most experiments add information only in a small area of this parameter space.

Computer simulations of SWNT growth on the other hand can provide insight into the nucleation and growth mechanisms based on a well-defined model system with precisely defined finely tunable conditions. However, until now, most molecular dynamics (MD) simulations following the *a priori* SWNT formation process on metal clusters employed variations of Brenner's computationally inexpensive reactive empirical bond order (REBO) potential,[8] which is a modified molecular mechanics (MM) potential and can therefore not account for the synergistic quantum-mechanical (QM) effect of increased stabilization with size increase of a π-conjugated system. In addition, the binding energy per carbon atom described by the REBO potential is the same for an aromatic six-membered or an antiaromatic eight-membered ring. The results from simulations such as those in Refs. 9–14 have therefore been questioned, one major point of criticism from experimentalists being "why do the grown SWNTs in the simulations contain many defects and do not possess a clearly developed (n,m) chirality?" Motivating our studies was the question "is this perhaps due to the neglect of electronic structure in the MM/MD simulations, and would a QM potential yield different cleaner structures?"

Due to the extraordinarily high computational cost, only few attempts have been reported on QM/MD simulations of SWNT nucleation and growth in the past. Two groups have performed first-principles MD simulations based on the Car-Parrinello molecular dynamics (CPMD) approach[15] applied to the nucleation process of a nanotube on transition-metal cluster.[16,17] Based on their limited simulation results, Gavillet *et al.*[16] suggested that the segregation of carbon linear chains and atomic rings on the surface of a liquidlike Co carbide cluster represents the first stage of the cap nucleation process, and they followed for 15 ps the incorporation of five carbon atoms into a preassembled half-fullerene cap attached to a Co metal surface. Raty *et al.*[17] studied early stages of SWNT growth on a hydrogen-terminated Fe_{55} cluster. In their work, the creation of a fullerenelike cap structure by continued supply of carbon atoms cluster was reported. However, upon closer inspection one finds that a nanodiamond "cap precursor" had been used as initial model system, which then spontaneously converted its sp^3 carbon framework into that of a single-layered sp^2 structure. Indeed, the same authors had already earlier shown that the sp^3 to sp^2 transformation spontaneously occurs on nanodiamond surfaces at high temperatures.[18] Therefore, their observations are irrelevant to the study of SWNT nucleation on metal nanoparticles. The question whether QM/MD simulations would substantially differ from the previous MM/MD simulations has not been answered by these two reported CPMD studies.

Very recently, we have performed QM/MD simulations employing the self-consistent-charge (SCC) density-functional tight-binding (DFTB) (Ref. 19) quantum chemical potential with finite electronic temperature,[20] which is com-

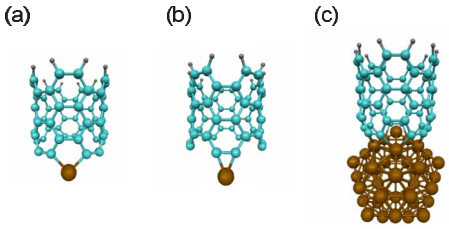

FIG. 1. (Color online) SCC-DFTB optimized structures of a (5,5) SWNT bonded to (a) and (b): an Fe atom and (c): an Fe_{55} cluster, where gray (small light gray sphere), cyan (light gray), and brown (dark gray) spheres represent hydrogen, carbon, and iron, respectively.

putationally less demanding than full CPMD simulations. Using the SCC-DFTB approach, we have demonstrated rapid continued growth of a seed SWNT attached to an Fe_{38} NP, when carbon atoms are supplied continuously to the metal-carbon boundary.[21] It was found that small linear C fragments at the Fe-C interface facilitate sidewall growth, and that heptagons are easier incorporated into the newly created carbon network compared to carbon-only simulations of fullerene formation.[22] In sharp contrast to REBO-based simulations, we never found incorporation of long-lasting four- or eight-membered rings into the sidewall, no kink deformations, and no long-lasting free valences on carbon present in the grown sidewalls. The near 1:1 ratio of pentagons vs heptagons we found should be suitable for Stone-Wales rearrangements to perfect hexagon networks upon further annealing. 1500 K seemed to represent a "sweet spot" in our simulations, as growth rates at 1000 and 2000 K were slightly reduced.[23] However, in that study we used a beforehand prepared SWNT fragment as initial model and did not address the details on the reactivity of feedstock carbons with carbon network on the NPs in more initial stage of SWNT nucleation. In the present simulations, we are focusing on this point by performing growth simulations based on the assumption that a small initial partial corannulenelike C_{20} fragment (a "cap fragment") somehow got assembled on an iron NP, as postulated by the "cap" growth mechanism in laser-evaporation or carbon-arc method.[24,25] QM/MD simulations of atomic carbon supply to the C-Fe interface or directly onto the cap are used to study in detail atomic-scale reaction dynamics between gas-phase C atoms and carbon-cap fragment on the iron cluster. The time evolution of polygonal ring components was investigated for a quantitative analysis of the dynamics.

II. ADHESION ENERGY

To demonstrate the reliability of the SCC-DFTB method for the energetics of iron NP-carbon interactions, we compare corresponding adhesion energies for Fe_n-(5,5) SWNT ($n=1$ and 55) complexes with those reported by Larsson *et al.*,[26] who recently employed density-functional theory (DFT) using the Perdew-Wang 1991 (PW91) functional with plane-wave basis sets for the exactly same systems. Figure 1 shows SCC-DFTB optimized geometries of these Fe_n-(5,5) SWNT complexes in their electronic ground states. In structures (a) and (b), a single iron atom is bound to the energetically most favorable sites at the end of the SWNT, respectively, while structure (c) represents a Fe_{55} cluster-(5,5) SWNT complex. Table I lists the adhesion energies at the PW91 and SCC-DFTB levels of theory. The adhesion energy was computed from the energy difference between the fully geometry-optimized Fe_n-SWNT complex and the separated SWNT and Fe_n systems. For the Fe_{55}-SWNT system (c), the adhesion energy was obtained by dividing the energy difference by 10, which is the number of unfilled bond valences at the rim of an open-ended (5,5) SWNT.[26] As can be seen in Table I, the DFTB calculation slightly underestimates atomic adhesion energies by ~20% (about 1 eV) compared to the PW91 results for structures (a) and (b). However, relative energy differences between structures (a) and (b) are very similar for both methods with the iron atom more strongly bound in the groove (a) rather than on the top of the rim of the SWNT (b). For the Fe_{55} cluster adhesion energy, even the absolute value of the SCC-DFTB adhesion energy in structure (c) is in excellent agreement with the first-principles PW91 result. Thus, it is fair to say that direct MD simulations based on the SCC-DFTB quantum chemical potential are of comparable quality to CPMD simulations.

TABLE I. Adhesion energies (eV/atom) for Fe_n-(5,5) SWNT clusters (a) and (b): with $n=1$ and (c): $n=55$, with the binding energy divided by 10. Corresponding structures are shown in Fig. 1. PW91 DFT values are quoted from Ref. 26.

	(a)	(b)	(c)
PW91	−6.24	−5.63	−1.82
SCC-DFTB	−5.17	−4.68	−1.86

III. SIMULATION DETAILS

The smallest possible cap fragment consists of a single pentagon surrounded by five hexagons, and we attach this corannulenelike C_{20} cap fragment on a truncated octahedron "magic"[27] fcc-Fe_{38} cluster (see Fig. 2). A fully developed and annealed cap structure should contain five more pentagons adjacent to the hexagons. We then supply carbon atoms to the metal-carbon cluster. Although C_2 and C_3 carbon species are also abundant in gas phase during laser ablation process,[28] we found that the lower reactivity of these species

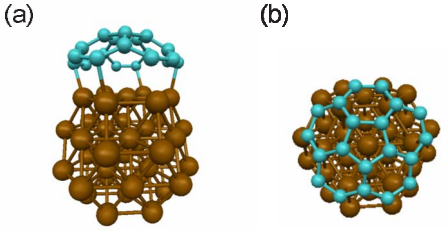

FIG. 2. (Color online) The $Fe_{38}C_{20}$ cluster for the nucleation simulation of a SWNT. (a) Side view and (b) top view. Cyan (light gray) and brown (dark gray) spheres represent carbon and iron atoms, respectively.

slows down the growth process, making such simulations at present unpractical. The choice of the relatively small size of Fe_{38} with ~7 Å diameter was largely determined by the high computational cost associated with the treatment of the metallic electronic structure. The electronic structure calculations were carried out using the SCC-DFTB with electronic temperature, using the iron-carbon DFTB parameters recently created by our group.[29] The electronic temperature allows the occupancy of each molecular orbital to change smoothly from 2 to 0 depending on its energy and effectively incorporates the open-shell nature of the system due near-degeneracy of iron *d* orbitals as well as carbon dangling bonds. We previously found that without electronic temperature the iron cluster is very low in reactivity and it does not promote the growth of nanotube. The benchmark calculations reported in Table I and Fig. 1 were performed with an electronic temperature of 1500 K, serving to improve SCC convergence. The "on the fly" electronic structure calculation during quantum chemical molecular dynamics simulations employed an electronic temperature of 10 000 K and the velocity Verlet integrator was used with a time step of 1 fs, while nuclear temperature was controlled using the Nose-Hoover chain thermostat.

At first, the starting structure shown in Fig. 2 was annealed using a nuclear temperature of 1500 K for 10 ps and then ten geometries and associated velocities were randomly extracted from the interval between 5 and 10 ps as starting points for subsequent carbon-supply simulations.

It is reasonable to consider that the rim area of the cap fragment is a primary reaction window to incorporate surface/subsurface carbon atoms. Along this line, we have implemented C-supply simulations around the C-Fe interface between the cap fragment and the iron cluster, identified as the carbon-supply simulation (i). We also explore multiple reaction pathways to the cap-to-tube transformation during SWNT growth by directly supplying C atoms onto the metal-bound cap fragment, identified as the carbon-supply simulation (ii). This carbon-supply simulation focuses on the reactivity of the entire carbon network of the metal-bound cap fragment with the gas-phase C atoms. Although the direct C atom bombardment on the cap fragment produces rather biased reaction events toward cap growth, the probability of reactions between gas-phase C atoms and cap fragment still should not be excluded for describing metal-bound SWNT growth in high-density C atoms.

The resulting trajectories are labeled alphabetically A–J for the carbon-supply simulation (i) and A'–J' for the simulation (ii). For both cases of (i) and (ii) a single C atom was supplied randomly every 0.6 ps with an incident energy of 0.052 eV, which corresponds to an atomic kinetic energy at 1500 K, either around the C-Fe interface for (i) or around the C_{20} fragment for (ii). The velocity vector of the incident carbon atom was directed toward an each time randomly chosen cap-constituent edge atom for simulation (i) or the cap-constituent atom for simulation (ii) in the growing carbon-cap fragment. The total number of supplied carbon atoms was 66 during the 40 ps simulations for both simulations (i) and (ii). The Cartesian coordinates of the full trajectories will become available.[30]

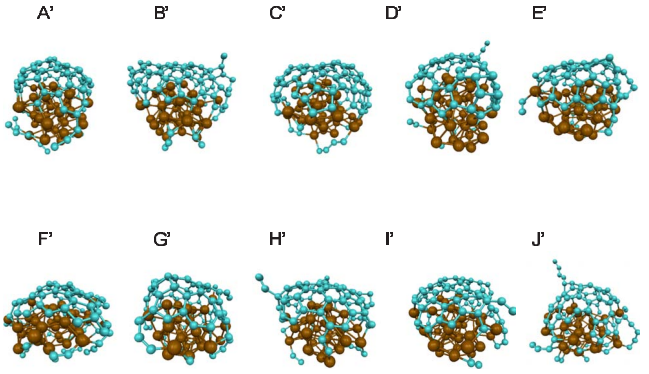

FIG. 3. (Color online) Final structures of ten trajectories after 40 ps growth simulation time where carbon atoms were supplied around the metal-carbon interface between the cap fragment and the iron cluster. The definition of colored spheres is given in Fig. 2.

IV. RESULTS AND DISCUSSION

Figure 3 shows snapshots of ten trajectories after 40 ps carbon-supply simulations around the C-Fe interface of the metal-carbon cluster [simulation (i)]. In almost all trajectories, carbon-cap fragments extend their carbon network by efficiently incorporating feedstock carbons at rim of the fragment. The resulting structures are typically characterized by cap-shaped network covering a large area of the iron surface, implying the formation of SWNT with diameters around ~11 Å, which is almost equivalent to the size of the extended iron cluster. During chemical vapor deposition (CVD) SWNT synthesis, most feedstock carbons are supplied by their surface/subsurface diffusion before reacting at the edge of the cap cluster. The structures obtained in simulation (i) indicate the development of larger cap structures that may further evolve into tubular structure on the iron surface. Lift-off of these larger caps was not observed within the time scale of our simulations. In order to realize tubular cluster formation, further supply of feedstock carbon atoms with longer simulation time would be necessary for constructing carbon sidewall.

Figure 4 shows snapshots of ten trajectories after 40 ps carbon-supply simulations targeted to the cap-constituent atoms [simulation (ii)]. In all the trajectories, the carbon-cap fragment increased in size and lifted off from the metal NP by rapidly incorporating the approaching incident carbon atoms. The resulting carbon network is constructed exclusively by sp^2-hybridized carbon atoms arranged in pentagons, hexagons, and heptagons. In particular trajectory D evolves to a clear rod-shaped SWNT structure of 10 Å length, and the diameter of the original carbon fragment is approximately maintained in agreement with the hypothetical "cap" growth mechanism.[24,25]

Such rapid formation of rod-shaped structure was never observed in simulation (i), indicating that simulation (ii) is more efficient than simulation (i) in terms of cap cluster growth. Within the relatively short simulation period, we did neither observe carbide formation nor the complete encapsulation of the metal NP by carbon. On the contrary, it is surprising how relatively "clean" the metal surface remains despite the fact that linear carbon fragments occasionally diffuse on its surface.

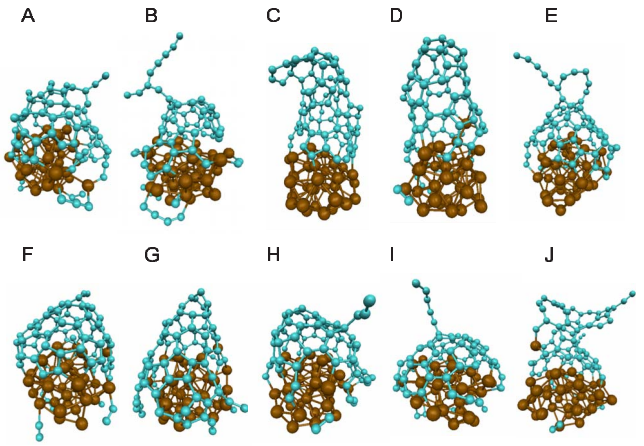

FIG. 4. (Color online) Final structures of ten trajectories after 40 ps growth simulation where carbon atoms were supplied to cap-constituent atoms. The definition of colored spheres is given in Fig. 2.

Figure 5 shows snapshots along the growth process of the SWNT structure in trajectory D and corresponding AVI movie is available in the EPAPS.[31] The simulation time "clock" was reset to zero at the moment of supply of the first incident carbon atom. At $t=0.5$ ps, this carbon atom was incorporated into the corannulenelike fragment and added onto a central pentagon/hexagon bond, expanding the structure to a hexagon/heptagon fused ring system. Such add atoms are reported to have autocatalytic activity for Stone-Wales transformations[32] and in the present case serve also frequently as anchoring points for the incorporation of additional supply carbon atoms. Surprisingly, during the course of the present simulations, the high density of add atoms and the cap fragment's resistance to accommodate resulting sp^3 defects led to continued major rearrangements of the existing sp^2-cap structures, with occasional occurrence of four-membered rings resulting from the interaction between

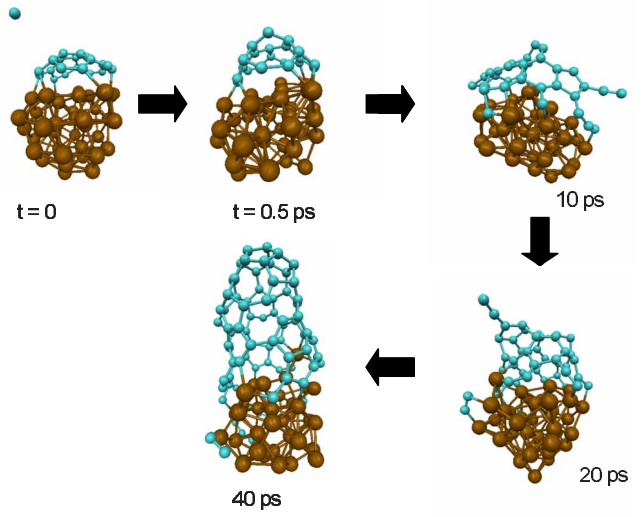

FIG. 5. (Color online) Snapshots along the growth process of a SWNT on an Fe_{38} cluster from a C_{20} cap, trajectory D. The definition of colored spheres is given in Fig. 2.

neighbored add atoms. Such highly strained rings however never remain stable but are rather fleeting intermediate structures, with subsequent rearrangements leading to either elimination of a C_2 unit or ring transformations. In general, we observe frequent dissociation or migration of C_2 units and linear carbon chains (see the snapshots at $t=10$ ps and $t=20$ ps in Fig. 5), which sometimes migrate along the restructuring cap fragment toward its edges where they become incorporated into the Fe-C interface region as newly created rings, or they react with each other to form a new segment, which slowly becomes incorporated into the existing cap fragment structure. The entire process is rather chaotic and a far cry from an ordered linear expansion of a growing sp^2 network. The coexistence of pentagons and heptagons in the hot SWNT structure is similar to the situation observed in our previous simulation of continued growth of SWNT.[21] The frequency of polyyne chain dissociation events seems to increase after the cap fragment evolved into a more stable cap and later capped rodlike structure. Other trajectories follow a very similar pattern of events but the resulting carbon caps are larger in diameter (for example, trajectory F) or carbon starts to encapsulate the metal NP (for example, trajectory I).

Figure 6 compares an average over ten trajectories obtained from simulation (i) with those from simulation (ii) regarding the ring-condensation dynamics. In both simulations, five-, six-, and seven-membered rings are found to be the primary components of the generated polygonal rings, while three- and four-membered rings are minor components. Interestingly, the numbers of primary polygonal rings (pentagons, hexagons, and heptagons) monotonically increase with time, while three- and four-membered rings never increase, which reflects their short-lived nature due to structural instability (in contrast to REBO simulations, for instance, Ref. 9). The final ring production ratio of five-, six-, and seven-membered rings is roughly 1:1:0.5 for both simulations (i) and (ii). The total sum of five-, six-, and seven-membered rings (all rings counted) was 21.0 and 18.1 for simulations (i) and (ii), respectively. The relatively large number of simulation (i) indicates reactive nature of edge carbon atoms.

From the analysis of the present simulations, we suggest that the early stage of a SWNT growth process starting from a C_{20} carbon-cap fragment can include multiple reaction paths to evolve into tubular form. The trajectories obtained in simulation (ii) especially suggest one possible reaction path composed of the following two stages. In *stage 1*, the cap fragment can directly react with feedstock carbon atoms to increase in size and lift off from the metal NP, evolving gradually into a more stable structure characterized by a larger sp^2-hybridized carbon network as a possible reaction path to extend its carbon network although surface/subsurface carbon atoms would more dominantly contribute to the extension of the cap fragment. Figure 7 illustrates suggested details of this cap fragment expansion stage. In step (a), an incident carbon atom reacts with the carbon-cap fragment and creates a deformed seven-membered ring, a typical add-atom structure. In step (b), the previously incorporated incident carbon is located in the protruded add-atom position in the cap fragment and a second incident carbon

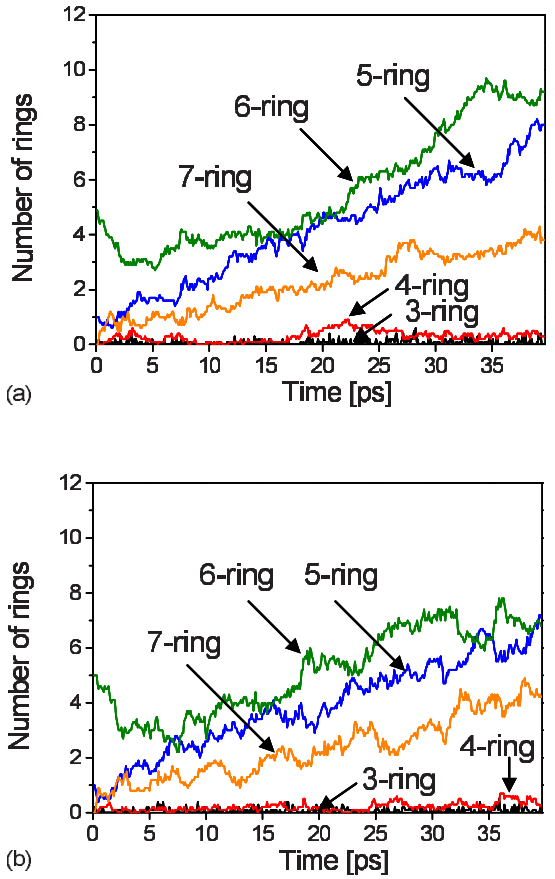

FIG. 6. (Color online) Ring-condensation dynamics during carbon-supply simulations. Black, three-membered ring; red, four-membered ring; blue, five-membered ring; green, six-membered ring; orange, seven-membered ring. (a) Carbon supply around the C-Fe interface between the cap fragment and the Fe_{38} cluster. (b) Carbon supply around the cap fragment on the Fe_{38} cluster.

atom approaches. In step (c), the second incident carbon is incorporated into the previously created seven-membered ring to form an eight-membered ring. The seven- and eight-membered rings are relatively unstable and easily evolve by rearrangement of the constituent carbon atoms as seen in steps (d) and (e), leading to the formation of smaller aromatic rings such as pentagons and hexagons in a growing cap fragment structure. As the cap fragment structure is extended in size, it gradually develops into a stable cap structure, becomes more inert and less reactive, and the process gradually commences (*stage 2*). At this stage, the reaction of feedstock carbon atoms occurs more dominantly in the metal-carbon boundary area (not on the inert cap), which promotes growth of the SWNT sidewall as we have described before for continued growth.[21]

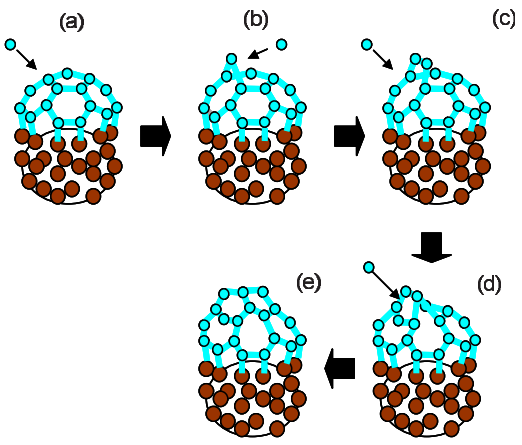

FIG. 7. (Color online) Schematic depictions of stage 1: development of the cap structure by carbon atom addition. Cyan (light gray) and brown (dark gray) spheres represent carbon and iron atoms, respectively.

Our simulations provide another insight into the evolution of a single pentagon cap fragment such as corannulene C_{20} to a fully formed chemically more inert SWNT cap structure that enables subsequent sidewall growth. (a) Carbon add atoms landing on the cap fragment induce almost instantaneously important structural rearrangements that will recover a smooth sp^2 network consisting of pentagons, hexagons, and heptagons via ring rearrangements as well as C_2 eliminations and migrations, (b) The instability of formally antiaromatic four- and eight-membered rings significantly contributes to the aforementioned cap fragment rearrangements, which is a process that cannot be observed in classical REBO-type MD simulations. (c) Pentagons as well as heptagons can survive on the order of at least about 50 ps and are important structural elements occurring the SWNT growth, which was also recently reported in an extensive quantum chemical study of assumed structures for growing nanotube sidewalls.[33] (d) Larger π-conjugated carbon caps are less reactive and become stabilized, while their edges maintain a high reactivity. Thus a stable cap will lift off from the metal particle and sidewall growth begins.

V. SUMMARY AND CONCLUSIONS

According to our QM/MD simulations, SWNT nucleation and growth on a metal cluster may actually take place in three stages: (A) formation of a cap fragment on the metal cluster (nucleation not observed yet), (B) expansion and lift-off of a carbon-cap fragment (cap formation), and (C) growth of SWNT "underneath" the cap structure (sidewall growth). In our previous study of continuous growth of prepared SWNT, we simulated stage C.[22,23] With the present model we were able to simulate stage B (corresponding to stage 1 in the present paper) and stage C (stage 2 above). Our finding of a rapid rod-shaped nanotube formation may explain reaction dynamics involved in the SWNT growth promoted by higher feeding rate of carbon in the nucleation stage of SWNT.[34]

Our previous and present simulations support the basic ideas of the hypothesized cap growth mechanism.[24,25] Still missing is an understanding of stage A, namely, how a carbon-cap fragment self-assembles on the surface of transition-metal cluster. Our various QM/MD simulation attempts so far suggest that this nucleation process should be very slow and may take much longer time than the following growth stages B and C. It looks like that for the nucleation stage the presence of a carbide layer on the metal nanopar-

ticle is required, as tight-binding grand canonical Monte Carlo simulations of SWNT nucleation on nickel suggest,[35] while growth clearly does not require the metal carbide formation. Studies along this line are ongoing in our laboratory.

We note that Yoshida *et al.*[6] reported liquidlike carbide NP formation and a complex dynamics of cap formation, subsequent cap destruction, and reappearance of the cap based on their recent ETEM observations. Although their experiment facilitated CVD synthesis, our simulations agree with their finding in the sense that cap formation involves frequent bond breaking and formation processes and is far from being an ordered linear process. Of course, their observations were made on the order of seconds, while we are only able to observe events on the order of picoseconds.

Insoluble behavior of carbon atoms inside the iron cluster observed in the present simulations is consistent with the results obtained from first-principles MD calculations in similar time scale. In close connection with this issue, we have recently demonstrated SWNT growth simulations using a capped (5,5)-SWNT portion attached to the Fe_{38} cluster with the addition of feedstock carbon on the iron surface. In these simulations, carbon diffusion dynamics was monitored in the course of 160 ps simulation time.[36] These simulations supplement description of long-time process of metal-carbon cluster where we have indeed observed that carbon atoms contribute to the extension of carbon sidewall through subsurface diffusion inside the iron cluster although the contribution of the surface carbon clusters were more dominant.

ACKNOWLEDGMENTS

This work was in part supported by a CREST (Core Research for Evolutional Science and Technology) grant in the Area of High Performance Computing for Multiscale and Multiphysics Phenomena from the Japan Science and Technology Agency (JST). One of the authors (S.I.) also acknowledges support by the Program for Improvement of Research Environment for Young Researchers from Special Coordination Funds for Promoting Science and Technology (SCF) commissioned by the Ministry of Education, Culture, Sports, Science and Technology (MEXT) of Japan. The simulations were performed in part using the computer resources at Academic Center for Computing and Media Studies (ACCMS) at Kyoto University.

*sirle@iar.nagoya-u.ac.jp
†morokuma@fukui.kyoto-u.ac.jp

[1] S. Maruyama, R. Kojima, Y. Miyauchi, S. Chiashi, and M. Kohno, Chem. Phys. Lett. **360**, 229 (2002).
[2] K. Hata, D. N. Futaba, K. Mizuno, T. Namai, M. Yumura, and S. Iijima, Science **306**, 1362 (2004).
[3] S. M. Bachilo, L. Balzano, J. E. Herrera, F. Pompeo, D. E. Resasco, and R. B. Weisman, J. Am. Chem. Soc. **125**, 11186 (2003).
[4] C. Lu and J. Liu, J. Phys. Chem. B **110**, 20254 (2006).
[5] S. Huang, M. Woodson, R. Smalley, and J. Liu, Nano Lett. **4**, 1025 (2004).
[6] H. Yoshida, S. Takeda, T. Uchiyama, H. Kohno, and Y. Homma, Nano Lett. **8**, 2082 (2008).
[7] S. Hofmann, R. Sharma, C. Ducati, G. Du, C. Mattevi, C. Cepek, M. Cantoro, S. Pisana, A. Parvez, F. Cervantes-Sodi, A. C. Ferrari, R. Dunin-Borkowski, S. Lizzit, L. Petaccia, A. Goldoni, and J. Robertson, Nano Lett. **7**, 602 (2007).
[8] D. W. Brenner, Phys. Rev. B **42**, 9458 (1990).
[9] F. Ding, K. Bolton, and A. Rosen, J. Phys. Chem. B **108**, 17369 (2004).
[10] F. Ding, K. Bolton, and A. Rosen, Comput. Mater. Sci. **35**, 243 (2006).
[11] F. Ding, A. Rosen, and K. Bolton, Carbon **43**, 2215 (2005).
[12] Y. Shibuta and S. Maruyama, Chem. Phys. Lett. **382**, 381 (2003).
[13] Y. Shibuta and S. Maruyama, Chem. Phys. Lett. **437**, 218 (2007).
[14] Y. Shibuta and S. Maruyama, Comput. Mater. Sci. **39**, 842 (2007).
[15] R. Car and M. Parrinello, Phys. Rev. Lett. **55**, 2471 (1985).
[16] J. Gavillet, A. Loiseau, C. Journet, F. Willaime, F. Ducastelle, and J.-C. Charlier, Phys. Rev. Lett. **87**, 275504 (2001).
[17] J. Y. Raty, F. Gygi, and G. Galli, Phys. Rev. Lett. **95**, 096103 (2005).
[18] J. Y. Raty, G. Galli, C. Bostedt, T. W. van Buuren, and L. J. Terminello, Phys. Rev. Lett. **90**, 037401 (2003).
[19] M. Elstner, D. Porezag, G. Jungnickel, J. Elsner, M. Haugk, T. Frauenheim, S. Suhai, and G. Seifert, Phys. Rev. B **58**, 7260 (1998).
[20] M. Weinert and J. W. Davenport, Phys. Rev. B **45**, 13709 (1992).
[21] Y. Ohta, S. Irle, Y. Okamoto, and K. Morokuma, ACS Nano **2**, 1437 (2008).
[22] S. Irle, G. Zheng, Z. Wang, and K. Morokuma, J. Phys. Chem. B **110**, 14531 (2006).
[23] Y. Ohta, Y. Okamoto, S. Irle, and K. Morokuma, J. Phys. Chem. C **113**, 159 (2009).
[24] H. Dai, A. G. Rinzler, P. Nikolaev, A. Thess, D. T. Colbert, and R. E. Smalley, Chem. Phys. Lett. **260**, 471 (1996).
[25] H. Kataura, Y. Kumazawa, Y. Maniwa, Y. Ohtsuka, R. Sen, S. Suzuki, and Y. Achiba, Carbon **38**, 1691 (2000).
[26] P. Larsson, J. A. Larsson, R. Ahuja, F. Ding, B. I. Yakobson, H. M. Duan, A. Rosen, and K. Bolton, Phys. Rev. B **75**, 115419 (2007).
[27] Q. M. Zhang, J. C. Wells, X. G. Gong, and Z. Y. Zhang, Phys. Rev. B **69**, 205413 (2004).
[28] S. Arepalli, C. D. Scott, P. Nikolaev, and R. E. Smalley, Chem. Phys. Lett. **320**, 26 (2000).
[29] G. Zheng, H. A. Witek, P. Bobadova-Parvanova, S. Irle, D. G. Mussaev, P. Prabhakar, and K. Morokuma, J. Chem. Theory Comput. **3**, 1349 (2007).
[30] http://kmweb.fukui.kyoto-u.ac.jp/nano
[31] See EPAPS Document No. E-PRBMDO-79-131915 for the AVI movie for trajectory B. For more information on EPAPS, see http://www.aip.org/pubservs/epaps.html.

[32] B. R. Eggen, M. I. Heggie, G. Jungnickel, C. D. Latham, R. Jones, and P. R. Briddon, Science **272**, 87 (1996).
[33] W. Zhu, A. Rosen, and K. Bolton, J. Chem. Phys. **128**, 124708 (2008).
[34] H. Qi, D. N. Yuan, and J. Liu, J. Phys. Chem. C **111**, 6158 (2007).
[35] H. Amara, C. Bichara, and F. Ducastelle, Phys. Rev. Lett. **100**, 056105 (2008).
[36] Y. Ohta, Y. Okamoto, S. Irle, and K. Morokuma, Carbon **47**, 1270 (2009).